Desantes, J.; Bermúdez, V.; López, JJ.; López-Pintor, D. (2017). Correlations for the ignition characteristics of six different fuels and their application to predict ignition delays under transient thermodynami conditions. Energy Conversion and Management. 152:124-135. doi:10.1016/j.enconman.2017.09.030

Correlations for the ignition characteristics of six different fuels and their application to predict ignition delays under transient thermodynamic conditions

José M. Desantes[a], Vicente Bermúdez[a], J. Javier López[a,*], Darío López-Pintor[a]

[a] *CMT-Motores Térmicos*
Universitat Politècnica de València
Camino de Vera, s/n. 46022 Valencia, SPAIN

Abstract

The ignition characteristics of six different fuels have been correlated as a function of the temperature, pressure, equivalence ratio and oxygen molar fraction in this investigation. More specifically, the ignition delay referred to cool flames, the high-temperature ignition delay and the critical concentrations and ignition times of HO_2 and CH_2O have been parameterized for n-dodecane, PRF0, PRF25, PRF50, PRF75 and PRF100. To do so, a wide database of ignition data of the aforementioned fuels has been generated by means of chemical simulations in CHEMKIN, solving a detailed mechanism for PRF mixtures and a reduced mechanism for n-dodecane. In fact, in-cylinder engine-like conditions reached in a Rapid Compression Expansion Machine (RCEM) have been replicated. The mathematical correlations have shown a relative deviation around 20% with the database in the low-temperature, low-pressure zone, which is the typical accuracy of usual cor-

*Corresponding author
Tel: +34 963 879 232. Fax: +34 963 877 659. E-mail: *jolosan3@mot.upv.es*

relations for the ignition delay. Finally, the ignition delay under transient conditions measured in the RCEM has been predicted by means of different integral methods coupled to both the proposed correlations and the generated database. I t has been found that deviations between the predictions obtained with the correlations or with the database are lower than 1%. This means that the correlations are accurate enough to predict the ignition time in spite of showing high deviation with the database, since the low-temperature, low-pressure zone has a minor contribution to the ignition delay.
Keywords: autoignition, ignition correlations, ignition delay, critical concentration

1. Introduction, justification and objective

Autoignition is a combustion mode with high relevance in propulsive systems for transport media and, more specifically, in reciprocating internal combustion engines. Standard Diesel CI-engines base their start of combustion on the autoignition of a fuel spray, while autoignition is an undesirable combustion mode in SI-engines, resulting in unacceptable pressures rise rates that can damage the engine [1]. Furthermore, most of the new advanced Low Temperature Combustion (LTC) modes are based on autoignition [2]. These modes combine lean equivalence ratios and high Exhaust Gas Recirculation (EGR) rates to reach low-emission, high-efficiency engines [3]. Thus, nowadays, autoignition has become a really interesting topic in the frame of internal combustion engines [4].

Autoignition characterization is a key procedure in control engine models. Despite the fact that the ignition can be well predicted by means of numer-

ical simulations with relatively low computational cost [5], the calculation time is too long to apply this methods in an Engine Control Unit (ECU) and, this way, controlling the engine in real time. Thus, the capability to characterize and even predict the ignition characteristics of different fuels is really interesting in the frame of engine control.

Mathematical correlations for the ignition delay are widely used in 0-D combustion models due to its simplicity and low calculation time. Pan et al. [6], for instance, correlated both ignition delays, referred to cool flames and referred to the high-temperature stage, for n-heptane and DME. Moreover, the NTC behavior and the temperature increment associated to cool flames were also parameterized. Besides, Desantes et al. [7] proposed expressions for the ignition delay of n-heptane and iso-octane in order to evaluate the chemical propagation velocity of a sequential autoignition process. Finally, it should be noted that the development of empirical correlations for the ignition delay is an extended methodology in rapid compression machine and shock tube studies, as the works of Kukkadapu et al. [8] and Weber et al. [9].

Furthermore, such mathematical correlations are usually linked to predictive methods to estimate the ignition delay under engine-like conditions. The most extended procedure is the classic Livengood & Wu integral method [10], which uses the ignition characteristics under constant thermodynamic conditions to predict the time of ignition under transient conditions as follows:

$$1 = \int_0^{t_i} \frac{1}{\tau} dt \tag{1}$$

where t_i represents the ignition delay of the process, while τ represents the ignition delay under constant conditions for each successive thermodynamic states reached in the process.

Several authors have used the Livengood & Wu integral method coupled to τ correlations to predict the ignition delay in combustion models for engine simulation and control. Hu et al. [11], for instance, used the Livengood & Wu integral method as a reaction progress variable to determine the instant and location of ignition for heterogeneous mixtures in CFD calculations. Furthermore, the integral method can be applied not only to SI-engines, but also to CI-engines. In fact, on the one hand, Zheng et al. [12] used the Livengood & Wu integral as the method to predict knock in 1-D engine cycle simulations. Experiments under knocking conditions were carried out in a turbocharged gasoline SI engine with cooled EGR and the knocking time were properly estimated by Eq. 1. On the other hand, Shahbakhti et al. [13] used the integral method as the way to control the ignition under HCCI conditions. The predictive method was validated by comparison to experimental data from a single cylinder engine in HCCI operation, in which the equivalence ratio, EGR level, engine speed, and intake temperature were varied for three different PRF blends with octane number values of 0, 10 and 20.

Different databases have been used to solve Eq. 1. For example, Choi et al. [14] trained an artificial neural network to predict ignition delays under constant thermodynamic conditions, τ, by means of the data obtained in a perfectly stirred reactor solving a detailed mechanism. The artificial neural network was linked to the Livengood & Wu integral method to predict

ignition delays under HCCI conditions.

However, the easiest way to implement Eq. 1 is by using mathematical correlations for the ignition characteristics under constant thermodynamic conditions. Rausen et al. [15] proposed a mean-value model to control HCCI engines, in which the start of combustion is given by the Livengood & Wu integral method. Empirical correlations were used to parameterize the ignition delay under constant conditions, while the model was validated using steady-state tests data from a gasoline engine. Besides, Zhou et al. [16] proposed mathematical correlations for the ignition delay under constant conditions, τ, based on simulations solving detailed chemical kinetic mechanisms for different fuels. The authors used these correlations to solve the Livengood & Wu integral method and predict the ignition under engine conditions. The comparison of predictions to 0-D simulations with detailed chemistry showed that the Livengood & Wu integral method is able to accurately reproduce the ignition characteristics at an insignificant computational cost, leading to a method to control the ignition in real time. Similar correlations have been proposed by Del Vescovo et al. [17] for PRF mixtures. The authors tested their correlations using the Livengood & Wu integral method and comparing the predictions to experimental HCCI heavy-duty engine data, obtaining a mean deviation of 1.5 CAD between predictions and experimental results. Finally, Hillion et al. [18] proposed an open-loop control strategy to improve the stability during transients of a conventional CI Diesel engine. The Livengood & Wu integral method was used coupled to Arrhenius-type correlations to adjust the injection time and avoid too violent ignitions. This strategy was implemented in a real engine, which was tested on a test bench and

on-board in a vehicle, and showed promising results in terms of combustion stability, pollutant emissions and noise.

The Livengood & Wu correlation has been recently used as an autoignition model for alternative fuels. Amador et al. [19], for instance, used the integral method to predict knock in an internal combustion engine fueled with Syngas. Their results showed that knock appears earlier if the methane number of the fuel increases. Besides, Kalghatgi et al. [20] tested the Livengood & Wu integral with five fuels that have different octane number values, sensitivities, and compositions, including ethanol blends. Predictions were compared to experiments in a single cylinder engine over a wide range of operating conditions, confirming that knock can be accurately predicted.

Desantes et al. [21, 22] proposed an alternative integral method to predict both ignition delays, the one referred to cool flames and the other one referred to the high-temperature stage of the process. Such method is based on the accumulation and consumption of chain carriers to determine the time at which the critical concentration occurs. More specifically, the method is composed by the two consecutive integrals:

$$1 = \frac{1}{[CC]_{crit,t=t_{CC}}} \int_0^{t_{CC}} \frac{[CC]_{crit}}{\tau_{CC}} dt \tag{2}$$

and

$$1 = \frac{1}{[CC]_{crit,t=t_{CC}}} \int_{t_{CC}}^{t_{HTHR}} \frac{[CC]_{crit}}{\tau_{HTHR} - \tau_{CC}} dt \tag{3}$$

where $[CC]_{crit}$ represents the critical concentration of chain carriers, while t_{CC} and τ_{CC} represent the ignition delay referred to such critical concentra-

tion under transient and constant conditions, respectively. Besides, t_{HTHR} and τ_{HTHR} represent the ignition delay referred to the high-exothermic stage under transient and constant conditions, respectively. The subscript 2 is used to distinguish these data to the corresponding ones referred to cool flames, which are usually denoted by the subscript 1. The method can be used to predict the occurrence of cool flames by solving Eq. 2 using HO_2 as chain carrier. Furthermore, the method allows to estimate the ignition delay referred to the high-temperature stage of the process by solving both Eqs. 2 and 3 using CH_2O as chain carrier.

Thus, the following ignition characteristics should be parameterized in order to implement the predictive method previously described in combustion models: ignition delays under constant conditions referred to HO_2, τ_{HO2}, to CH_2O, τ_{CH2O}, and to the high-temperature stage, τ_{HTHR}, and critical concentrations of HO_2, $[HO_2]_{crit}$, and CH_2O, $[CH_2O]_{crit}$. Furthermore, the ignition delay under constant conditions referred to cool flames, τ_{LTHR}, has been additionally correlated. According to the authors' knowledge, correlations for the critical concentration of chain carriers, as well as for the ignition delay referred to such critical concentration (for both HO_2 and/or CH_2O), are not available in the literature, which makes impossible the implementation of the method proposed by Desantes et al. [21, 22].

These ignition characteristics are intended to be correlated for six different fuels in this work. The tested fuels cover the whole octane number scale (from -40 for n-dodecane, to 100 for iso-octane), which allows to implement the proper correlation for a wide range of fuels and combustion modes. To do so, a wide database of ignition delays and critical concentrations of

chain carriers is generated covering most of the operation range present in internal combustion engines. Finally, the ignition delay under transient conditions has been predicted using the integral method proposed by Desantes et al., indicated above, coupled to both correlations and database, and both predictions have been compared to each other.

The structure of the paper is the following: first, the methodological approach is described, including the generation of the database, the development of the correlations and the range of validity of each of them. Afterwards, results are discussed, including the accuracy of the proposed correlations and their application to predict the ignition delay. Finally, the conclusions of this study are shown.

2. Methodological approach

The methodology followed in this investigation is detailed in this section. More specifically, the generation of a database of ignition delays and critical concentrations is explained, as well as the algorithm used for the fitting procedure of the proposed correlations.

2.1. Database generation

Different ignition delays and critical concentrations under constant thermodynamic conditions have been obtained by means of numerical simulations in CHEMKIN. The experimental temperature and pressure evolutions obtained in an RCEM have been used as guidelines to generate the database, since the usual in-cylinder conditions reached in an engine wants to be covered. More specifically, the following experiments have been taken into account:

- Experiments carried out with n-heptane and iso-octane by Desantes et al. [21].
- Experiments carried out with PRF25, PRF50 and PRF75 by Desantes et al. [22].
- Experiments carried out with n-dodecane by Desantes et al. [23].

The RCEM used in the previously cited investigation is briefly described in order to facilitate the reader to understand how the experimental conditions are representative of engines. Stroke and clearance volume can be modified in the RCEM in order to reproduce different engine geometrical characteristics, resulting in the capability of working with a wide range of compression ratios. Besides, the engine speed can be simulated by changing the compression velocity. The experimentation piston that compresses the test sample into the combustion chamber is 84 mm in bore and includes a cylindrical bowl, 46 mm in bore and 17 mm in depth. The piston position is measured by an AMO LMK102 incremental position sensor with 0.01 mm of resolution. This way, the piston position and, consequently, the combustion chamber volume are known. The initial temperature, as well as the temperature of the walls, are controlled by a PID regulator that acts over an electrical 80 W heater located in the bowl and two more spire-shape electrical heaters (600 W each) located in the liner. the control loop is possible by measuring the temperature by three thermocouples located in the liner, in the piston and in the bowl, respectively. A Kistler 6045A uncooled piezoelectric pressure sensor located in the cylinder head (-45 pC/bar of sensitivity) is coupled to a Kistler 5018 charge amplifier for the measurement of the in-cylinder pres-

sure. Besides, the filling of both, the combustion chamber and the driving gas volume are controlled by three Wika piezoresistive pressure sensors (0.01 bar of resolution). Finally, a common rail system that includes a 7-hole nozzle implemented in a BOSCH solenoid-commanded injector that is controlled by a EFS IPod power driving module forms the injection system. A Yokogawa DL850V system composed by one 10 MHz-12 bits module and five more 1 MHz-16 bits modules with two channels each acts as acquisition system, in which 10 MHz are fixed as acquisition frequency. Such a high acquisition frequency is mandatory to be able to measure the electrical pulses of the incremental position sensor. However, both, in-cylinder and injection pressures are recorded at 1 MHz. A heated external tank (up to 5204 K by three electrical heaters, 1200 W each) is used for the generation of the synthetic air, which is produced by mixing N_2, CO_2 and O_2 according to their partial pressures. Moreover, H_2O can be added thanks to a syringe pump. Vacuum is created before generating each mixture and before filling the RCEM to ensure the no contamination in this tank, nor in the combustion chamber. Finally, the exact composition of the synthetic mixture is measured by gas chromathography in a Rapid Refinery Gas Analyser from Bruker (450-GC) in order to ensure the correct reproduction of the experiments.

Figure 1 shows the move law of the RCEM compared to an engine. It can be seen that both paths are really similar around TDC. It can be seen that the RCEM piston path is really similar to an engine in the range approx. form -72 CAD to +45 CAD around TDC. More specifically, the equivalent engine correspond to a virtual engine that has the same stroke and compression ratio, and the same compression time (engine speed).

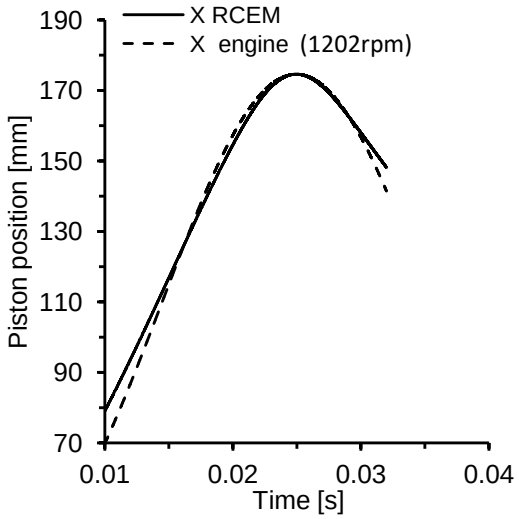

Figure 1: Move law of the RCEM compared to an engine.

Fig. 2 shows the experimental conditions tested in the three references cited above. More specifically, the in-cylinder thermodynamic conditions reached during the compression stroke (pressure versus temperature path) are plotted. It can be seen that a wide range of engine operating point is taken into account with such test matrix. Furthermore, the following equivalence ratios, ϕ, and oxygen molar fractions, X_{O_2}, have been tested:

- N-heptane and iso-octane: $\phi \in [0.3 - 0.6]$, $X_{O_2} \in [0.105 - 0.21]$
- PRF25, PRF50, PRF75 and n-dodecane: $\phi \in [0.3 - 0.7]$, $X_{O_2} \in [0.16 - 0.21]$

The tested range depends on the characteristics of the experimental facility used for each fuel. Besides, it should be noted that the previous ranges define the limits of validation of the correlations proposed in this investigation.

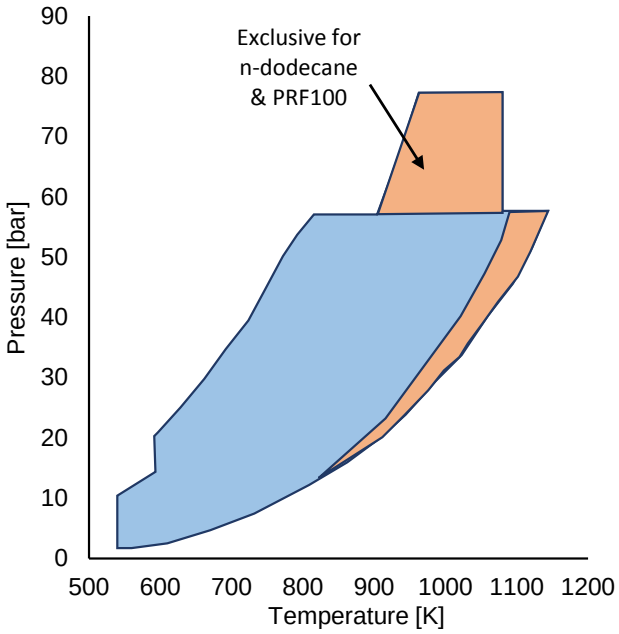

Figure 2: In-cylinder pressure and temperature reached in the RCEM experiments.

The temperature and pressure evolutions of each specific experiment have been discretized in (T, P) values each $\Delta t = 10^{-5} s$, which is the minimum resolution of in-cylinder pressure measurements. Moreover, temperatures below 550 K have not been taken into account, since they lead to too long ignition delays that will have no effect in the computation of the predictive integral method (Eqs. 2 and 3).

As said before, CHEMKIN is the software used to obtain the different ignition delays and critical concentrations. On the one hand, the Curran's kinetic mechanism is used for the PRF blends [24–26]. This mechanism consists of 1034 species and 4238 reactions, and includes the chemical kinetics of the two hydrocarbons used as reference in the octane number scale: n-heptane and iso-octane. On the other hand, the reduced mechanism from Lawrence Livermore National Laboratory (LLNL) [27] is used for n-dodecane. This mechanism consists of 163 species and 887 reactions and it has been generated starting form the detailed mechanism for n-alkanes of LLNL, which is composed by 2885 species and 11754 reactions [28]. In fact, the detailed mechanism for n-dodecane is avoided due to the high computational cost of generating the database by solving it. It should be mentioned that both chemical kinetic mechanisms have been validated in the working range versus experimental measurements in [22] and [23].

Each (T, P) value is simulated for a certain equivalence ratio, oxygen molar fraction and fuel in a homogeneous closed reactor (perfectly stirred reactor, PSR), which works with constant pressure and uses the energy equation to solve the temperature temporal evolution. This model is the most appropriate to obtain ignition delays at constant pressure and temperature

conditions [29], since working with constant pressure corrects, somewhat, the over-prediction of the pressure which is typical of this kind of reactor [30]. Besides, the maximum waiting time for the autoignition of the mixture has been set to 30 s, which provides enough accuracy in the calculations.

Specifically, the following information is included in the database:

- Operating conditions, which includes fuel, temperature, T, pressure, P, equivalence ratio, ϕ, and oxygen molar fraction, X_{O_2}.

- Ignition delay referred to cool flames, τ_{LTHR}, which is defined as the time at which the peak of low-temperature heat release rate (heat release rate caused by cool flames) occurs.

- Ignition delay referred to the high-temperature stage of the process, τ_{HTHT}, which is defined as the time at which the maximum heat release rate occurs.

- Ignition delay and critical concentration referred to HO_2, τ_{HO2} and $[HO_2]_{crit}$, respectively. The critical concentration of HO_2 is assumed as the maximum concentration of such species and it has been demonstrated to be a good tracer for cool flames. The ignition delay referred to HO_2 is defined as the time at which the critical concentration of HO_2 occurs.

- Ignition delay and critical concentration referred to CH_2O, τ_{CH2O} and $[CH_2O]_{crit}$, respectively. The critical concentration of CH_2O is assumed as the maximum concentration of such species and it has been demonstrated to be a good tracer for the end of the NTC zone. The ignition

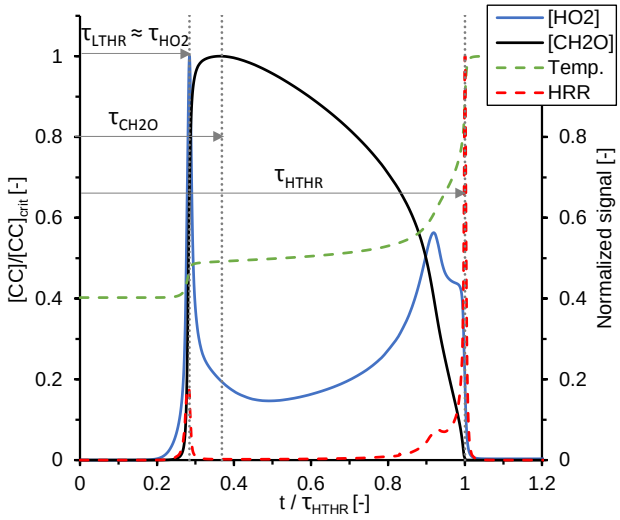

Figure 3: Simulation results of a PSR for n-dodecane at 750 K and 18 bar, the equivalence ratio and the oxygen molar fraction are 0.5 and 0.21, respectively.

delay referred to CH_2O is defined as the time at which the critical concentration of CH_2O occurs.

Fig. 3 shows the result of a simulation carried out in a PSR. The different variables included in the database are identified in the figure. Simulations performed in CHEMKIN were processed in an in-house developed Matlab routine to extract the information that composes the database.

2.2. Correlations development

The proposed correlations are based on the chain carriers accumulation rate up to reach the critical concentration, which defines the ignition delay. Starting from the conservation of species equation for the concentration of chain carriers and assuming a homogeneous mixture under static conditions (null convective and diffusive terms), a characteristic time of the process up

to reach the critical concentration will be an estimator of the ignition delay, and it can be obtained as follows:

$$\frac{d[CC]}{dt} = \dot{\omega}_{CC} \rightarrow \tau \approx \frac{[CC]_{crit}}{\dot{\omega}_{CC}} \tag{4}$$

where $[CC]$ represents the concentration of chain carriers and the source term, $\dot{\omega}_{CC}$, represent a global reaction rate.

In this study, the ignition delay is assumed to be composed by two different terms: one that dominates under medium-to-high temperature conditions, and another one that dominates under low-temperature conditions. It should be noted that, according to Fig. 2, an ignition delay term that characterizes the high-temperature conditions where the uni-molecular fuel decomposition is relevant (above 1500 K) has not to be taken into account. Therefore, the total ignition delay will be equal to the sum of the previous two, and it can be parameterized (taking into account Eq. 4 and the dependence of the reaction rates on the working conditions) as follows:

$$\begin{aligned}\tau &= \frac{[CC]_{crit}}{k_{i,1}\,[O_2]^{a_1}\,[F]^{b_1}} + \frac{[CC]_{crit}}{k_{i,2}\,[O_2]^{a_2}\,[F]^{b_2}} = \\ &= \frac{[CC]_{crit}}{A_1 T^{n_1} P^{m_1} exp\left(\frac{-E_{a,1}}{RT}\right)[O_2]^{a_1}\,[F]^{b_1}} + \frac{[CC]_{crit}}{A_2 T^{n_2} P^{m_2} exp\left(\frac{-E_{a,2}}{RT}\right)[O_2]^{a_2}\,[F]^{b_2}}\end{aligned} \tag{5}$$

where $[O_2]$ and $[F]$ represent the concentration of reactants: oxidizer and fuel, respectively; and k_i represent the specific reaction rate of the process. The expression to characterize the specific reaction rate can be deduced by the collision theory for bi-molecular reactions [31], where A is the coefficient that

imposes the units of k_i, n and m are dimensionless experimental coefficients, E_a is the activation energy and R is the universal gas constant. This expression coincides with the extended Arrhenius' empirical expression, which can be extrapolated to reactions with an order different from two. Following a qualitative interpretation of the extended Arrhenius' expression, AT^nP^m depends on the reactant molecules and it is an estimator of the collision frequency, meanwhile the exponential term is an estimator of the percent of collisions that have energy enough to react.

Eq. 5 can be rewritten assuming that variations of the critical concentration are much smaller than variations of the reaction rate. Moreover, the equivalence ratio, ϕ, is assumed as an estimator of the fuel concentration, $[F]$, and the normalized oxygen molar fraction, $X_{O_2}/X_{O_2,atm}$ (where $X_{O_2,atm}$=0.21), is assumed as an estimator of the oxygen concentration, $[O_2]$. Thus:

$$\begin{aligned}\tau =& K_1 T^{-n_1} P^{-m_1} exp\left(\frac{T_{a,1}}{T}\right)\left(\frac{X_{O_2}}{0.21}\right)^{-a_1}\phi^{-b_1}+ \\ &+ K_2 T^{-n_2} P^{-m_2} exp\left(\frac{T_{a,2}}{T}\right)\left(\frac{X_{O_2}}{0.21}\right)^{-a_2}\phi^{-b_2}\end{aligned} \tag{6}$$

where $T_a = E_a/R$ represents the activation temperature, in Kelvin, which together with K, n, m, a and b should be fitted to match the database.

Regarding the critical concentration of chain carriers, the following statistical correlations have been proposed:

$$[HO_2]_{crit} = aT^2 + b\phi^c\left(\frac{X_{O_2}}{0.21}\right)^d P^e T + f\phi^g\left(\frac{X_{O_2}}{0.21}\right)^h P^i + j \tag{7}$$

and

$$\frac{1}{[CH_2O]_{crit}} = \frac{1}{C_1 + C_2} + \frac{1}{C_3} \tag{8}$$

where C_1, C_2 and C_3 are:

$$C_1 = a_1 \phi^{b_1} \left(\frac{X_{O_2}}{0.21} \right)^{c_1} P^{d_1} exp\left(\frac{-e_1}{T} \right) \tag{9}$$

$$C_2 = a_2 \phi^{b_2} \left(\frac{X_{O_2}}{0.21} \right)^{c_2} P^{d_2} exp\left(\frac{-T}{e_1} \right) \tag{10}$$

$$C_3 = a_3 \phi^{b_3} \left(\frac{X_{O_2}}{0.21} \right)^{c_3} P^{d_3} exp\left(\frac{T}{e_3} \right) \tag{11}$$

where a, b, c, d, e, f, g, h, i and j are calibration constants that should be fitted to match the database.

The correlations for the critical concentration of chain carriers are not based on any physical model, but they are based on statistis. Therefore, their validity is not guaranteed for operating conditions out of the tested range, i.e., extrapolations of Eqs. 7 and 8 can lead to unexpected wrong results.

2.3. Fitting procedure

The different calibration constants of Eqs. 6, 7 and 8 have been fitted to match the database by means of the Levenberg-Marquardt algorithm, which tries to solve a non-linear least squares problem. More specifically,

the algorithm minimize the deviation function $S = \sum (y - f(x_i, \beta))^2$, where y represents the data from the database and $f(x_i, \beta)$ is the correlation to fit, which depends on the input variables, $x_i \in \{T, P, \phi, X_{O_2}\}$, and on the calibration constants, β. To do so, the following system of equations is solved by applying an iterative process:

$$\left(J^T J + \lambda diag\left(J^T J\right)\right) \delta = J^T \left(y - f(x_i, \beta)\right) \tag{12}$$

where $J = \partial f(x_i, \beta) / \partial \beta$ is the Jacobian matrix of the correlation. δ represents the variation of β, so that $\beta_{j+1} = \beta_j + \delta$. Finally, λ is the Marquardt parameter, which is a non-negative damping factor that is adjusted in each iteration and that controls the nature of the algorithm. If the objective function S decreases rapidly, a smaller value of λ is used, bringing the algorithm closer to the Gauss-Newton algorithm. Otherwise, λ is increased, bringing the algorithm closer to the gradient-descent algorithm. The λ variation is defined by an initial value, a maximum value and a scale factor, which are equal to 0.01, 120 and 20 in this study, respectively.

Starting from an initial condition, β_0, the variation of the calibration constants, δ, can be obtained from Eq. 12, leading to an iterative process by which the new variation of the calibration constants is calculated using the previous β vector. Two different criteria have been imposed to end the iterative procedure. On the one hand, the process ends if δ/β reaches a value small enough (0.01% in this study). On the other hand, the process ends if the relative variation of the objective function S (the deviation function) is small enough (0.001% in this study).

3. Results and discussion

The results of the fitting procedure are shown in this section, including statistic parameters to quantify the quality of the correlations. Furthermore, the resulting formulas have been coupled to Eqs. 2 and 3 to predict the ignition delay. Finally, predictions from the database and from the proposed correlations are compared to each other.

3.1. Mathematical correlations

Figs. 4, 5, 6 and 7 to the left show database and correlations versus temperature for the different ignition delays of n-heptane: referred to cool flames, τ_{LTHR}, referred to the high-temperature stage, τ_{HTHR}, referred to a critical concentration of HO_2, τ_{HO2}, and referred to a critical concentration of CH_2O, τ_{CH2O}, respectively. N-heptane has been selected as the fuel to show because it presents the worst correlations. The mean relative deviation, $\bar{\xi}$, the value of which can be seen also in the figures, has been calculated as follows:

$$\bar{\xi} = \frac{1}{N} \sum \frac{|\tau_{correlation} - \tau_{database}|}{\tau_{database}} 100 \tag{13}$$

Figs. 4, 5, 6 and 7 to the right directly compare the correlations (in the ordinate axis) to the database (in the abscissas axis) for n-heptane. The Pearson's coefficient of determination, R^2, is also plotted in the figures.

Special attention should be paid to Fig. 7. The transition between the low and high-temperature mechanisms causes a sudden change in the evolution of τ_{CH2O}, the behavior of which is defined by the chemical kinetic mechanism

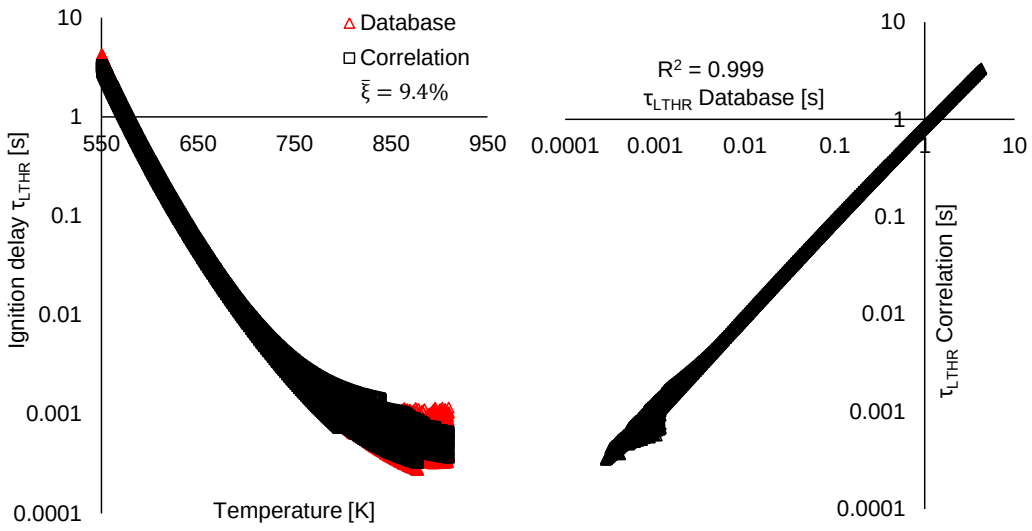

Figure 4: Ignition delay referred to cool flames, τ_{LTHR}, from the database and from the proposed correlation for n-heptane. Left.- Variation with temperature. Right.- Comparison between data.

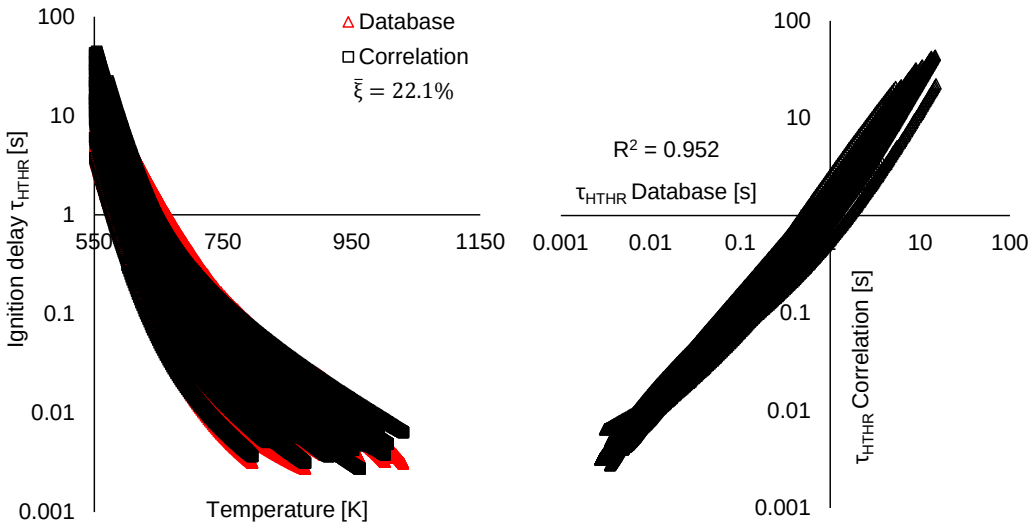

Figure 5: Ignition delay referred to the high-temperature stage, τ_{HTHR}, from the database and from the proposed correlation for n-heptane. Left.- Variation with temperature. Right.- Comparison between data.

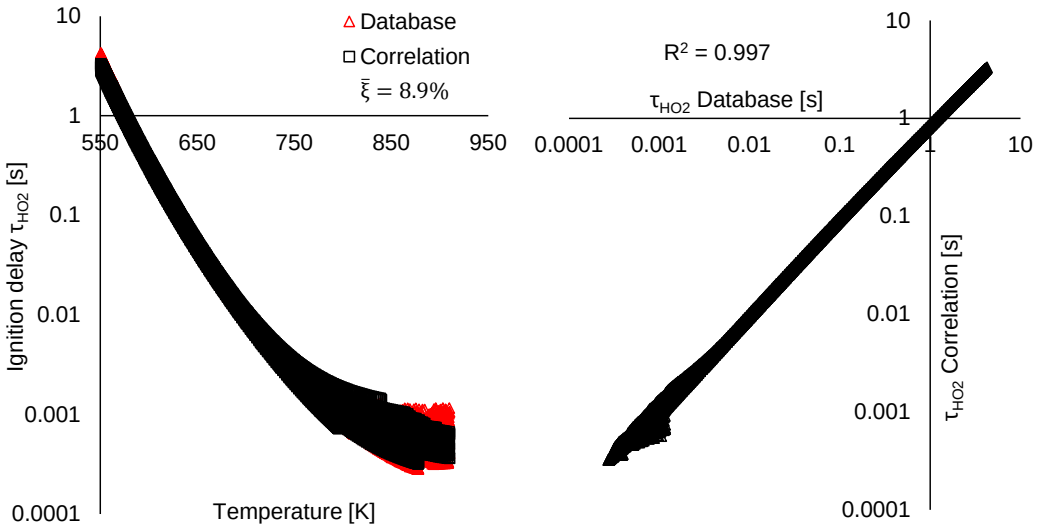

Figure 6: Ignition delay referred to the critical concentration of HO_2, τ_{HO2}, from the database and from the proposed correlation for n-heptane. Left.- Variation with temperature. Right.- Comparison between data.

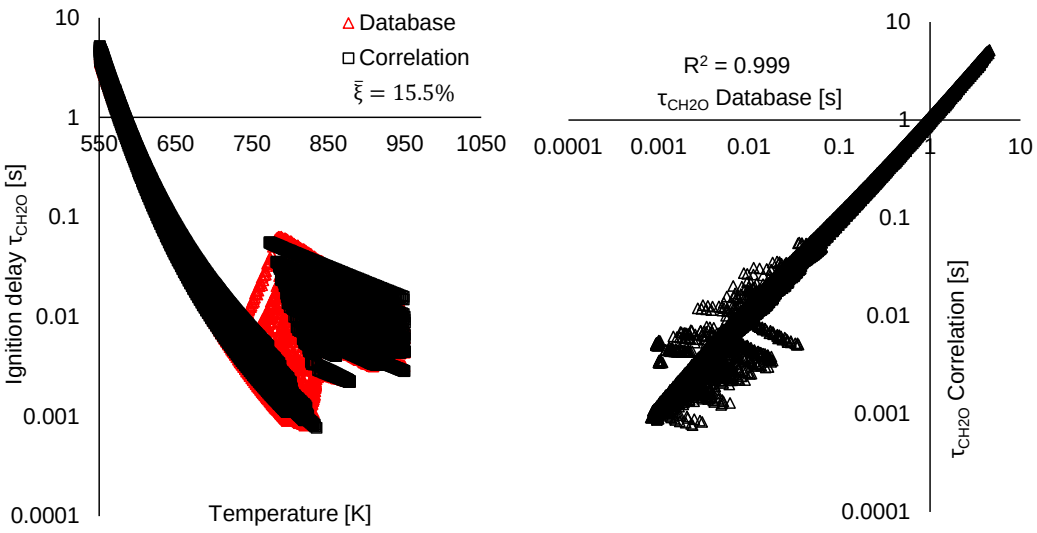

Figure 7: Ignition delay referred to the critical concentration of CH_2O, τ_{CH2O}, from the database and from the proposed correlation for n-heptane. Left.- Variation with temperature. Right.- Comparison between data.

used to generate the database. Thus, this transition leads to discontinuities in the τ_{CH2O} function, which are reproduced by a piecewise correlation. The transition temperature is parameterized as follows:

$$T_{transition} = aP^b\phi^c\left(\frac{X_{O_2}}{0.21}\right)^d \tag{14}$$

Therefore, if the temperature is lower than the transition temperature, the ignition delay referred to a critical concentration of CH_2O is defined by Eq. 6, whereas the following correlation is proposed for τ_{CH2O} in case of having a temperature value above the transition temperature:

$$\tau_{CH2O} = K_3T^{-n_3}P^{-m_3}exp\left(\frac{T_{a,3}}{T}\right)\left(\frac{X_{O_2}}{0.21}\right)^{-a_3}\phi^{-b_3} \quad if \quad T > T_{transition} \tag{15}$$

In fact, discrepancies in Fig. 7 to the right are caused by the assumption of a piecewise function. It should be noted that this behavior has not be seen for n-dodecane, since the transition between temperature regimes depends on the chemical kinetic mechanism and the one used for n-dodecane seems to have a smoother transition.

Tables 1 to 6 summarize the fitted value of the calibration constants for all fuels and all ignition delays. Furthermore, Table 13 summarizes the mean relative deviation, $\bar{\xi}$, and the Pearson's coefficient of determination, R^2, for all fuels and all ignition delays.

Figs. 8 and 9 to the left show database and correlations versus temperature for the different critical concentrations of n-heptane: referred to HO_2 and referred to CH_2O, respectively. The mean relative deviation, $\bar{\xi}$, has been

		N-dodecane					
		K_i	n_i	m_i	$T_{a,i}$	a_i	b_i
τ_{LTHR}	i=1	$4.40{\cdot}10^{-9}$	-1.356	0.930	4003	1.372	0.382
	i=2	$4.66{\cdot}10^{-6}$	1.869	0.074	13267	0.128	0.078
τ_{HTHR}	i=1	$8.89{\cdot}10^{-2}$	0.641	1.128	2473	2.184	1.416
	i=2	$4.20{\cdot}10^{-8}$	0.685	0.211	11465	1.153	1.119
τ_{HO2}	i=1	$2.00{\cdot}10^{-8}$	-1.200	0.954	250	0.500	0.500
	i=2	$4.66{\cdot}10^{-6}$	1.869	0.074	13267	0.128	0.078
τ_{CH2O}	i=1	$2.50{\cdot}10^{-8}$	-1.390	1.316	3203	1.596	1.741
	i=2	$1.55{\cdot}10^{-9}$	0.543	0.079	13186	0.137	0.083
	i=3	-	-	-	-	-	-
		a	**b**	**c**	**d**		
$T_{transition}$		-	-	-	-		

Table 1: Calibration constants for the ignition delay correlations of n-dodecane.

PRF0

		K_i	n_i	m_i	$T_{a,i}$	a_i	b_i
τ_{LTHR}	i=1	7.736	0.336	1.093	-3846	1.472	0.138
	i=2	$2.70{\cdot}10^{-5}$	2.115	0.024	13647	0.215	0.135
τ_{HTHR}	i=1	$2.24{\cdot}10^{-2}$	0.059	1.441	2317	2.012	1.020
	i=2	$6.80{\cdot}10^{-12}$	0.010	0.819	15039	2.564	2.199
τ_{HO2}	i=1	7.736	0.336	1.093	-3846	1.472	0.138
	i=2	$2.70{\cdot}10^{-5}$	2.115	0.024	13647	0.215	0.135
τ_{CH2O}	i=1	$3.34{\cdot}10^{-6}$	0.371	0.590	7910	0.770	0.410
	i=2	$6.20{\cdot}10^{-7}$	2.270	0.043	16349	0.344	0.277
	i=3	18896	1.282	1.641	-1992	2.223	0.968

	a	**b**	**c**	**d**
$T_{transition}$	735.6	$4.05{\cdot}10^{-2}$	$1.01{\cdot}10^{-2}$	$6.15{\cdot}10^{-2}$

Table 2: Calibration constants for the ignition delay correlations of PRF0.

PRF25

		K_i	n_i	m_i	$T_{a,i}$	a_i	b_i
τ_{LTHR}	i=1	$1.48{\cdot}10^{-4}$	0.485	0.163	4000	0.651	0.178
	i=2	$4.13{\cdot}10^{-6}$	2.223	0.020	15448	0.173	0.112
τ_{HTHR}	i=1	$4.47{\cdot}10^{-3}$	-0.227	1.514	2188	2.224	1.466
	i=2	$7.48{\cdot}10^{-7}$	2.679	0.152	18083	0.383	0.259
τ_{HO2}	i=1	$9.50{\cdot}10^{-10}$	-1.200	0.954	125	1.500	1.500
	i=2	$7.23{\cdot}10^{-6}$	2.023	0.020	14448	0.173	0.112
τ_{CH2O}	i=1	$2.22{\cdot}10^{-4}$	1.007	0.542	7776	0.517	0.356
	i=2	$1.65{\cdot}10^{-6}$	2.180	$1.91{\cdot}10^{-4}$	15754	0.179	0.119
	i=3	4.990	0.382	1.571	-78.53	1.779	1.123

	a	**b**	**c**	**d**
$T_{transition}$	669.2	$5.50{\cdot}10^{-2}$	$-1.54{\cdot}10^{-2}$	$-2.90{\cdot}10^{-3}$

Table 3: Calibration constants for the ignition delay correlations of PRF25.

PRF50

		K_i	n_i	m_i	$T_{a,i}$	a_i	b_i
τ_{LTHR}	i=1	$1.45{\cdot}10^{-6}$	-1.416	1.221	592.4	1.602	0.416
	i=2	$1.13{\cdot}10^{-5}$	2.430	0.012	15815	0.353	0.142
τ_{HTHR}	i=1	18.88	0.773	1.464	928.8	3.695	1.383
	i=2	$3.61{\cdot}10^{-5}$	2.136	0.142	14142	0.383	0.259
τ_{HO2}	i=1	$1.45{\cdot}10^{-6}$	-1.416	1.221	592.4	1.602	0.416
	i=2	$1.13{\cdot}10^{-5}$	2.430	0.012	15815	0.353	0.142
τ_{CH2O}	i=1	$3.69{\cdot}10^{-5}$	-0.288	0.776	3297	1.415	0.473
	i=2	$1.66{\cdot}10^{-6}$	2.151	0.015	15901	0.387	0.157
	i=3	1388.5	1.387	1.449	882.2	3.010	1.154

	a	**b**	**c**	**d**
$T_{transition}$	657.7	$5.45{\cdot}10^{-2}$	$-1.17{\cdot}10^{-2}$	$-4.30{\cdot}10^{-3}$

Table 4: Calibration constants for the ignition delay correlations of PRF50.

PRF75

		K_i	n_i	m_i	$T_{a,i}$	a_i	b_i
τ_{LTHR}	i=1	$1.00{\cdot}10^{-6}$	-1.104	1.045	2836	0.762	0.449
	i=2	$3.70{\cdot}10^{-6}$	2.260	0.016	16067	0.203	0.157
τ_{HTHR}	i=1	$3.90{\cdot}10^{-3}$	-0.102	1.470	3649	1.797	1.364
	i=2	$2.22{\cdot}10^{-5}$	2.288	0.086	15116	0.386	0.307
τ_{HO2}	i=1	$1.00{\cdot}10^{-6}$	-1.104	1.045	2836	0.762	0.449
	i=2	$3.70{\cdot}10^{-6}$	2.260	0.016	16067	0.203	0.157
τ_{CH2O}	i=1	$3.54{\cdot}10^{-5}$	-0.135	0.783	4586	1.104	0.661
	i=2	$1.81{\cdot}10^{-6}$	2.147	$1.85{\cdot}10^{-2}$	16069	0.216	0.167
	i=3	261.0	1.255	1.511	2243	1.658	1.218

	a	**b**	**c**	**d**
$T_{transition}$	606.1	$6.29{\cdot}10^{-2}$	$-2.68{\cdot}10^{-2}$	$-1.50{\cdot}10^{-3}$

Table 5: Calibration constants for the ignition delay correlations of PRF75.

PRF100

		K_i	n_i	m_i	$T_{a,i}$	a_i	b_i
τ_{LTHR}	i=1	570.7	0.336	1.093	-3846	1.472	0.138
	i=2	$1.81 \cdot 10^{-5}$	2.261	0.074	15462	0.299	0.205
τ_{HTHR}	i=1	-	-	-	-	-	-
	i=2	$1.48 \cdot 10^{-4}$	1.294	0.833	14266	0.971	0.703
τ_{HO2}	i=1	570.7	0.336	1.093	-3846	1.472	0.138
	i=2	$1.81 \cdot 10^{-5}$	2.261	0.074	15462	0.299	0.205
τ_{CH2O}	i=1	-	-	-	-	-	-
	i=2	$9.65 \cdot 10^{-5}$	1.383	0.813	15169	0.863	0.670
	i=3	$1.70 \cdot 10^{-10}$	-0.579	0.454	11437	1.074	0.720

	a	**b**	**c**	**d**
$T_{transition}$	566.8	$6.37 \cdot 10^{-2}$	$-3.52 \cdot 10^{-2}$	$-1.80 \cdot 10^{-3}$

Table 6: Calibration constants for the ignition delay correlations of PRF100.

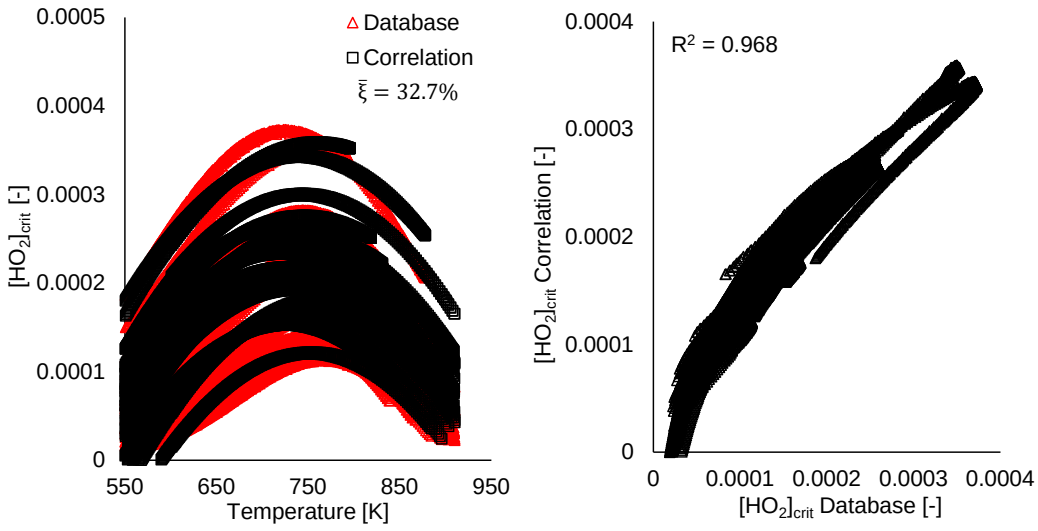

Figure 8: Critical concentration of HO_2 from the database and from the proposed correlation for PRF0. Left.- Variation with temperature. Right.- Comparison between data.

calculated analogously to Eq. 13 and its value is also presented in the figures. The same figures to the right directly compare the correlations (in the ordinate axis) to the database (in the abscissas axis) for n-heptane. The Pearson's coefficient of determination, R^2, is also plotted in the figures.

Finally, Tables 7 to 12 summarize the fitted value of the calibration constants for all fuels and the critical concentration of both species. Furthermore, Table 13 summarizes the mean relative deviation, $\bar{\xi}$, and the Pearson's coefficient of determination, R^2, for all fuels and both species, when comparing the predicted and the database critical concentration.

3.2. Application for the ignition delay prediction

The proposed correlations have been linked to Eqs. 2 and 3 in order to predict the ignition delay under transient conditions. The in-cylinder tem-

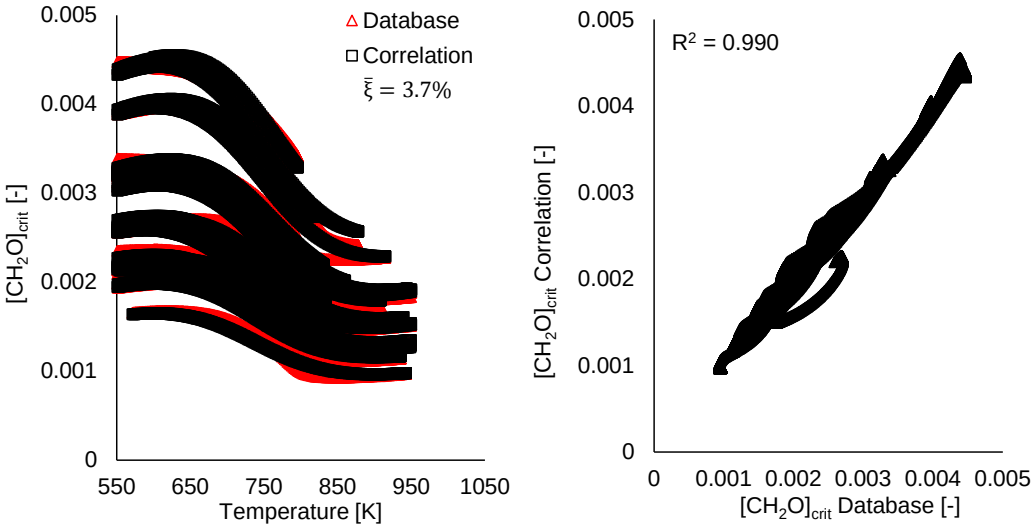

Figure 9: Critical concentration of CH_2O from the database and from the proposed correlation for PRF0. Left.- Variation with temperature. Right.- Comparison between data.

		N-dodecane				
		a_i	b_i	c_i	d_i	e_i
$[CH_2O]_{crit}$	i=1	$2.72{\cdot}10^{-2}$	0.800	1.066	-0.121	1000
	i=2	72760	1.077	1.077	0.026	50.85
	i=3	$3.50{\cdot}10^{-3}$	1.357	1.450	-0.053	1000
$[HO_2]_{crit}$	-	$-3.55{\cdot}10^{-9}$	$4.36{\cdot}10^{-6}$	-0.188	-0.042	0
		f	g	h	i	j
	-	$-6.50{\cdot}10^{-4}$	-0.853	-0.549	$5.63{\cdot}10^{-3}$	0

Table 7: Calibration constants for the critical concentration correlations of n-dodecane.

		PRF0				
		a_i	b_i	c_i	d_i	e_i
$[CH_2O]_{crit}$	i=1	$2.17{\cdot}10^{-2}$	0.950	0.950	0.048	1000
	i=2	7276	-1.090	-1.144	-0.537	52.00
	i=3	$6.20{\cdot}10^{-3}$	0.991	0.998	0.013	1000
$[HO_2]_{crit}$	-	$-6.39{\cdot}10^{-9}$	$8.23{\cdot}10^{-6}$	-0.039	$-6.60{\cdot}10^{-3}$	0.031
		f	g	h	i	j
	-	$-7.20{\cdot}10^{-3}$	-0.050	-0.038	0.024	$4.99{\cdot}10^{-3}$

Table 8: Calibration constants for the critical concentration correlations of PRF0.

		PRF25				
		a_i	b_i	c_i	d_i	e_i
$[CH_2O]_{crit}$	i=1	$1.29{\cdot}10^{-2}$	1.237	1.118	0.028	1000
	i=2	72760	2.591	1.144	0.172	49.82
	i=3	$5.10{\cdot}10^{-3}$	0.921	1.158	$9.60{\cdot}10^{-3}$	1000
$[HO_2]_{crit}$	-	$-5.24{\cdot}10^{-9}$	$7.01{\cdot}10^{-6}$	-0.120	-0.123	0
		f	g	h	i	j
	-	$-1.86{\cdot}10^{-3}$	-0.369	-0.431	$4.72{\cdot}10^{-3}$	0

Table 9: Calibration constants for the critical concentration correlations of PRF25.

		PRF50				
		a_i	b_i	c_i	d_i	e_i
$[CH_2O]_{crit}$	i=1	$1.39{\cdot}10^{-2}$	0.871	1.318	0.054	1000
	i=2	8532	0.908	1.144	0.516	50.00
	i=3	$5.00{\cdot}10^{-3}$	1.000	2.178	$1.59{\cdot}10^{-2}$	1000
$[HO_2]_{crit}$	-	$-4.90{\cdot}10^{-9}$	$6.04{\cdot}10^{-6}$	-0.053	-0.124	0.040
		f	g	h	i	j
	-	$-8.60{\cdot}10^{-3}$	-0.043	-0.110	$2.13{\cdot}10^{-2}$	$7.12{\cdot}10^{-3}$

Table 10: Calibration constants for the critical concentration correlations of PRF50.

		PRF75				
		a_i	b_i	c_i	d_i	e_i
$[CH_2O]_{crit}$	i=1	$2.14{\cdot}10^{-2}$	1.371	1.318	0.054	1000
	i=2	24253	2.591	1.144	0.172	49.82
	i=3	$3.70{\cdot}10^{-3}$	0.921	1.158	$7.59{\cdot}10^{-2}$	1000
$[HO_2]_{crit}$	-	$-3.89{\cdot}10^{-9}$	$4.57{\cdot}10^{-6}$	-0.062	-0.033	0.047
		f	g	h	i	j
	-	$-2.68{\cdot}10^{-3}$	-0.100	-0.078	$5.41{\cdot}10^{-2}$	$1.51{\cdot}10^{-3}$

Table 11: Calibration constants for the critical concentration correlations of PRF75.

		PRF100				
		a_i	b_i	c_i	d_i	e_i
$[CH_2O]_{crit}$	i=1	$5.51 \cdot 10^{-2}$	1.067	1.014	-0.071	1458
	i=2	5000	0.940	0.966	0.022	40.00
	i=3	10.00	0.940	0.966	$2.17 \cdot 10^{-2}$	157.2
$[HO_2]_{crit}$	-	$-1.59 \cdot 10^{-9}$	$1.89 \cdot 10^{-6}$	-0.020	$-6.71 \cdot 10^{-3}$	0.038
		f	g	h	i	j
	-	$-6.47 \cdot 10^{-3}$	$-6.34 \cdot 10^{-3}$	$-5.26 \cdot 10^{-3}$	$7.20 \cdot 10^{-3}$	$5.96 \cdot 10^{-3}$

Table 12: Calibration constants for the critical concentration correlations of PRF100.

		τ_{LTHR}	τ_{HTHR}	τ_{HO2}	τ_{CH2O}	$[HO_2]_{crit}$	$[CH_2O]_{crit}$
N-dodecane	$\bar{\xi}$ [%]	25.8	18.3	14.6	10.9	6.2	3.9
	R^2	0.999	0.995	0.999	0.983	0.974	0.986
PRF0	$\bar{\xi}$ [%]	9.4	22.1	8.9	15.5	32.7	3.7
	R^2	0.999	0.952	0.997	0.999	0.968	0.990
PRF25	$\bar{\xi}$ [%]	11.1	17.3	13.7	7.5	8.9	4.5
	R^2	0.999	0.995	0.999	0.999	0.968	0.979
PRF50	$\bar{\xi}$ [%]	10.8	13.3	10.8	5.5	21.0	6.3
	R^2	0.999	0.989	0.999	0.999	0.973	0.990
PRF75	$\bar{\xi}$ [%]	6.7	14.3	7.1	4.2	7.1	3.3
	R^2	0.999	0.997	0.999	0.999	0.975	0.984
PRF100	$\bar{\xi}$ [%]	10.1	18.3	9.6	16.0	20.8	6.9
	R^2	0.999	0.934	0.999	0.964	0.908	0.967

Table 13: Mean relative deviation, $\bar{\xi}$, and Pearson's coefficient of determination, R^2, for the tested fuels and the proposed correlations.

perature and pressure evolutions obtained from the experiments described in Section 2.1 have been applied to the predictive method, and Eqs. 2 and 3 have been solved using both the database and the correlations.

An example of the predictive procedure is shown in Fig. 10. The experimental conditions are used to determine the ignition delay and critical concentration functions under constant thermodynamic conditions. Finally, Eqs. 2 and 3 are computed resulting in an estimation of the ignition delay of the process. Obviously, there is a certain deviation between predictions and experiments, independently of using information from the database or from the correlations. However, the accuracy of the predictions will not be shown in this paper, since it has been discussed by Desantes et al. in [21–23].

Fig. 11 shows all ignition delay predictions referred to cool flames (left) and to the high-temperature stage (right). Predictions obtained from the database are plotted in the abscissas axis, whereas those obtained from the correlations are plotted in the ordinate axis. Ignition delays of PRF0 are larger than those of PRF25, PRF50 and PRF75 because PRF0 has been tested at lower oxygen molar fractions. Besides, ignition delays of PRF100 reach similar values than those of PRF0 because PRF100 has been tested at higher temperatures and pressures. The mean relative deviation between both predictions has been calculated analogously to Eq. 13, as well as the Pearson's coefficient of determination for each fuel and each ignition stage. Finally, deviations and R^2 values are summarized in Table. 14. It should be noted that cool flames cannot be identified for the cases performed with PRF75 nor PRF100. Thus, only predictions referred to the high-temperature stage can be calculated.

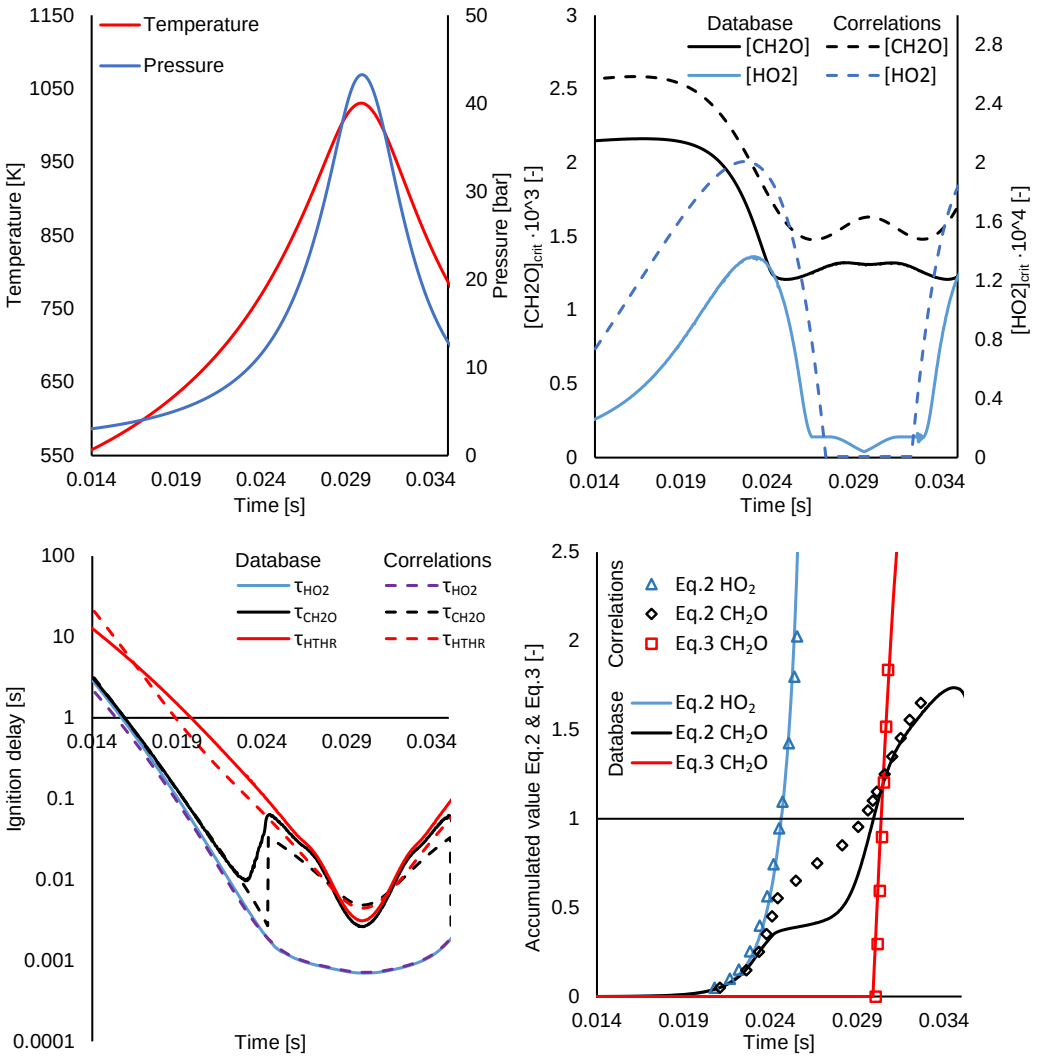

Figure 10: Predictive procedure applied to an experiment fueled with PRF0. Initial temperature 458 K, initial pressure 1.4 bar, compression ratio 14, equivalence ratio 0.4, oxygen molar fraction 0.126. Top left.- in-cylinder temperature and pressure signals. Top right.- Critical concentration functions. Bottom left.- Ignition delay functions. Bottom right.- Eqs. 2 and 3.

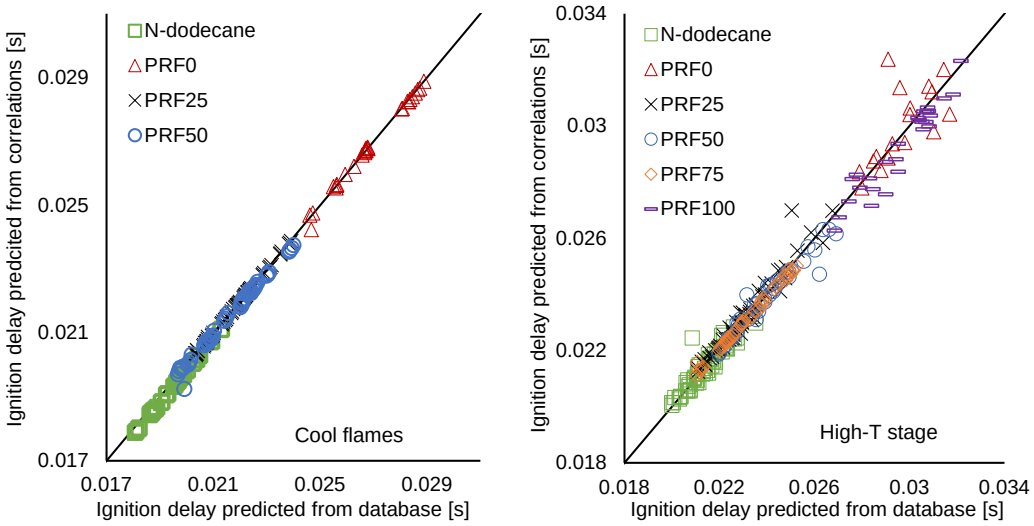

Figure 11: Ignition delay predictions computed from the correlations versus those obtained from the chemical kinetic database. All fuels are plotted. Left.- Cool flames. Right.- High-temperature stage.

	Cool flames		**High temperature**	
	$\bar{\xi}$ [%]	R^2	$\bar{\xi}$ [%]	R^2
N-dodecane	0.949	0.983	0.919	0.916
PRF0	0.193	0.962	2.439	0.635
PRF25	0.131	0.983	0.974	0.956
PRF50	0.496	0.976	0.854	0.949
PRF75	-	-	0.414	0.976
PRF100	-	-	1.598	0.642

Table 14: Deviations and R^2 values for all fuels and both ignition events, cool flames and the high-temperature ignition.

It can be seen that correlations lead to very similar predicted ignition delays than chemical kinetic mechanisms in spite of showing high deviations (≈20%) for the ignition delays and critical concentrations under constant conditions. This is caused by the accumulation behavior of Eqs. 2 and 3, which mainly occurs in a narrow range of temperatures. In fact, as shown by Fig. 10, the 75% of the final values of Eqs. 2 and 3 are accumulated in ≈15% of the ignition delay time. Therefore, correlations should be accurate only in such time interval, which coincides with the medium-temperature regime. Thus, low or high-temperature conditions are not relevant to predict the autoignition and correlations can show high deviations at such regimes without leading to wrong predictions.

4. Conclusions

Mathematical correlations have been proposed to characterize different ignition delays and critical concentrations of six fuels that covers the octane number scale from -40 (n-dodecane) to 100 (iso-octane). More specifically, ignition delays under constant conditions referred to HO_2, τ_{HO2}, to CH_2O, τ_{CH2O}, and to the high-temperature stage, τ_{HTHR}, and critical concentrations of HO_2, $[HO_2]_{crit}$, and CH_2O, $[CH_2O]_{crit}$ have been parameterized. Furthermore, the ignition delay under constant conditions referred to cool flames, τ_{LTHR}, has been also correlated. The fitting procedure is based on the application of the Levenberg-Marquardt algorithm to a wide database of ignition characteristics obtained by solving two different chemical kinetic mechanisms in CHEMKIN, covering a wide range of operating conditions present in internal combustion engines.

The following conclusions can be deduced from this study:

- Ignition delays, τ, have been parameterized taken into account two different contributions: one related to the low-temperature oxidation and another one related to the medium-to-high temperature regime.

- The proposed correlations show a deviation of around 20% compared to the database, which is a similar accuracy than the one presented by other formulas available in the literature.

- However, differences of only 1% have been obtained between the correlations and the database when they are used to predict the ignition delay under transient thermodynamic conditions. Thus, correlations are valid to be used in predictive integral methods despite of their high deviation when they are directly compared to the database.

- Correlations can be used to predict the ignition delay because most of the contribution to the integral predictive methods are performed in a narrow range of temperatures and pressure. Thus, correlations should be accurate only in a narrow range of operating conditions.

Acknowledgements

The authors would like to thank different members of the CMT-Motores Térmicos team of the Universitat Politècnica de València for their contribution to this work. The authors would also like to thank the Spanish Ministry of Education for financing the PhD. Studies of Darío López-Pintor (grant FPU13/02329). This research has been partially funded by FEDER and the Spanish Government through project TRA2015-67136-R.

Notation

CAD	Crank Angle Degrees
CC	Referred to chain carriers
$[CC]_{crit}$	Critical concentration of chain carriers
CI	Compression ignition
CFD	Computational Fluid Dynamics
Ea	Activation energy for the Arrhenius expression
ECU	Engine Control Unit
EGR	Exhaust Gas Recirculation
f	Correlation function
$[F]$	Fuel concentration
$HCCI$	Homogeneous Charge Compression Ignition
k_i	Specific reaction rate
$LLNL$	Lawrence Livermore National Laboratory
LTC	Low Temperature Combustion

N	Number of samples
NTC	Negative Temperature Coefficient
P	Pressure
PRF	Primary Reference Fuel
PSR	Perfectly Stirred Reactor
R	Universal gas constant
R^2	Pearson's coefficient of correlation
$RCEM$	Rapid Compression-Expansion Machine
SI	Spark ignition
t	Time
T	Temperature
T_a	Activation temperature
t_i	Ignition delay under transient thermodynamic conditions
$t_{i,2}$	Ignition delay referred to the high-temperature stage of the process
$t_{i,CC}$	Ignition delay referred to a critical concentration of chain carriers
x_i	Input variables vector
X_{O2}	Oxygen molar fraction
y	Data vector from the chemical kinetic database
β	Calibration constants vector
δ	β variation
$\bar{\xi}$	Mean relative deviation between database and correlation results
ϕ	Working equivalence ratio

λ	Marquardt parameter
τ	Ignition delay under constant conditions of pressure and temperature
τ_{LTHR}	Ignition delay under constant conditions referred to cool flames
τ_{HTHR}	Ignition delay under constant conditions referred to the high-temperature stage
τ_{CC}	Ignition delay under constant conditions referred to a critical concentration of chain carriers
$\dot{\omega}$	Global reaction rate

References

[1] J.J. Lopez, R. Novella, J. Valero-Marco, G. Coma, and F. Justet. Evaluation of the potential benefits of an automotive, gasoline, 2-stroke engine. *SAE Technical Paper*, 2015-01-1261, 2015.

[2] J. Benajes, S. Molina, A. Garcia, and J. Monsalve-Serrano. Effects of direct injection timing and blending ratio on RCCI combustion with different low reactivity fuels. *Energy Conversion and Management*, 99:193–209, 2015.

[3] T. Li, D. Wu, and M. Xu. Thermodynamic analysis of EGR effects on the first and second law efficiencies of a boosted spark-ignited direct-injection gasoline engine. *Energy Conversion and Management*, 70:130–138, 2013.

[4] J. Benajes, J.V. Pastor, A. Garcia, and J. Monsalve-Serrano. An experimental investigation on the influence of piston bowl geometry on RCCI performance and emissions in a heavy-duty engine. *Energy Conversion and Management*, 103:1019–1030, 2015.

[5] K. Bahlouli, U. Atikol, R.K. Saray, and V. Mohammadi. A reduced mechanism for predicting the ignition timing of a fuel blend of natural-gas and n-heptane in HCCI engine. *Energy Conversion and Management*, 79:85–96, 2014.

[6] J. Pan, P. Zhao, C.K. Law, and H. Wei. A predictive livengood-wu correlation for two stage ignition. *International Journal of Engine Research*, 17:825–835, 2016.

[7] J. M. Desantes, J. J. Lopez, J.M. Garcia-Oliver, and D. Lopez-Pintor. A phenomenological explanation of the autoignition propagation under HCCI conditions. *Fuel*, In press, 2017.

[8] Goutham Kukkadapu, Kamal Kumar, Chih-Jen Sung, Marco Mehl, and William J. Pitz. Experimental and surrogate modeling study of gasoline ignition in a Rapid Compression Machine. *Combustion and Flame*, 159:3066–3078, 2012.

[9] Bryan W. Weber, Kamal Kumar, Yu Zhang, and Chih-Jen Sung. Autoignition of n-butanol at elevated pressure and low-to-intermediate temperature. *Combustion and Flame*, 158:809–819, 2011.

[10] J.C. Livengood and P.C. Wu. Correlation of autoignition phenomena in internal combustion engines and rapid compression machines. *Symposium (International) on Combustion*, 5:347–356, 1955.

[11] Z. Hu, B.L.M.T. Somers, R.F. Cracknell, and D. Bradley. Investigation of the livengood?wu integral for modelling autoignition in a high-pressure bomb. *Combustion Theory and Modelling*, 20:77–98, 2016.

[12] L. Chen, T. Li, T. Yin, and B. Zheng. A predictive model for knock onset in spark-ignition engines with cooled EGR. *Energy Conversion and Management*, 87:946–955, 2014.

[13] M. Shahbakhti, R. Lupul, and C. R. Koch. Predicting HCCI autoignition timing by extending a modified knock-integral method. *SAE Paper no. 2007-01-0222*, 2007.

[14] Y. Choi and J.Y. Chen. Fast prediction of start-of-combustion in HCCI with combined artificial neural networks and ignition delay model. *Proceedings of the Combustion Institute*, 30:2711–2718, 2005.

[15] D.J. Rausen, A.G. Stefanopoulou, J.M. Kang, J.A. Eng, and T.W. Kuo. A mean-value model for control of homogeneous charge compression ignition HCCI engines. *Journal of Dynamic Systems, Measurement, and Control*, 127:355–362, 2005.

[16] A. Zhou, T. Dong, and B. Akih-Kumgeh. Simplifying ignition delay prediction for homogeneous charge compression ignition engine design and control. *International Journal of Engine Research*, 17:957–968, 2016.

[17] D. DelVescovo, S. Kokjohn, and R. Reitz. The development of an ignition delay correlation for prf fuel blends from prf0 (n-heptane) to prf100 (iso-octane). *SAE Technical Paper 2016-01-0551*, 2016.

[18] M. Hillion, J. Chauvin, and N. Petit. Control of highly diluted combustion in diesel engines. *Control Engineering Practice*, 19:1274–1286, 2011.

[19] G. Amador, J. Duarte-Forero, A. Rincon, A. Fontalvo, A. Bula, R. Vasquez-Padilla, and W. Orozco. Characteristics of auto-ignition in internal combustion engines operated with gaseous fuels of variable methane number. *Journal of Energy Resources Technology*, 139, 2017.

[20] G. Kalghatgi, K. Morganti, I. Algunaibet, M. Sarathy, and R. Dibble. Knock prediction using a simple model for ignition delay. *SAE Technical Paper 2016-01-0702*, 2016.

[21] J. M. Desantes, V. Bermudez, J. J. Lopez, and D. Lopez-Pintor. A new method to predict high and low-temperature ignition delays under transient thermodynamic conditions and its experimental validation using a Rapid Compression-Expansion Machine. *Energy Conversion and Management*, 123:512–522, 2016.

[22] J. M. Desantes, V. Bermudez, J. J. Lopez, and D. Lopez-Pintor. Experimental validation of an alternative method to predict high and low-temperature ignition delays under transient thermodynamic conditions for PRF mixtures using a Rapid Compression-Expansion Machine. *Energy Conversion and Management*, 129:23–33, 2016.

[23] J. M. Desantes, V. Bermudez, J. J. Lopez, and D. Lopez-Pintor. Sensitivity analysis and validation of a predictive procedure for high and low-temperature ignition delays under engine conditions for n-dodecane using a Rapid Compression-Expansion Machine. *Energy Conversion and Management*, 145:64–81, 2017.

[24] H.J. Curran, P. Gaffuri, Pitz W.J, and C.K. Westbrook. A comprehensive modeling study of n-heptane oxidation. *Combustion and Flame*, 114:149–177, 1998.

[25] H.J. Curran, P. Gaffuri, Pitz W.J, and C.K. Westbrook. A comprehensive modeling study of iso-octane oxidation. *Combustion and Flame*, 129:253–280, 2002.

[26] H.J. Curran, W.J. Pitz, C.K. Westbrook, C.V. Callahan, and F.L. Dryer.

Oxidation of automotive primary reference fuels at elevated pressures. *Proceedings of the Combustion Institute*, 27:379–387, 1998.

[27] T. Lu, M. Plomer, Z. Luo, S.M. Sarathy, W.J. Pitz, S. Som, and D.E. Longman. Directed relation graph with expert knowledge for skeletal mechanism reduction. *7th US National Combustion Meeting*, Paper 1A03,:203–248, 2011.

[28] S.M. Sarathy, C.K. Westbrook, M. Mehl, W.J. Pitz, C. Togbe, P. Dagaut, H. Wang, M.A. Oehlschlaeger, U. Niemann, K. Seshadri, P.S. Veloo, C. Ji, F.N. Egolfopoulos, and T. Lu. Comprehensive chemical kinetic modeling of the oxidation of 2-methylalkanes from c7 to c20. *Combustion and Flame*, 158:2338–2357, 2011.

[29] F. Payri, X. Margot, S. Patouna, F. Ravet, and M. Funk. Use of a single-zone thermodynamic model with detailed chemistry to study a natural gas fueled Homogeneous Charge Compression Ignition engine. *Energy Conversion and Management*, 53:298–304, 2012.

[30] P. Redon. *Modelling of the nitogen oxides formation process applicable to several diesel combustion modes*. PhD thesis, Universitat Politecnica de Valencia, Valencia (Spain), 2013.

[31] R. H. Petrucci, W. S. Harwood, and F. G. Herring. *General Chemistry*. Prentice Hall, 2001.